INVESTIGATING THE SPATIAL AND TEMPORAL INTERACTIONS IN RESTING-STATE FMRI WITH TOTAL ACTIVATION

F. Işık Karahanoğlu [1,2,3], *Dimitri Van De Ville*[1,2]

[1] Institute of Bioengineering, Ecole Polytechnique Fédérale de Lausanne (EPFL),Switzerland
[2]Department of Radiology and Medical Informatics, University of Geneva (UNIGE), Switzerland
[3]Department of Psychiatry, University of Geneva (UNIGE), Switzerland

ABSTRACT

Resting-state functional magnetic resonance imaging (fMRI) has become an important tool to study the spontaneous brain fluctuations. Especially, in terms of network analysis, the intrinsic brain activations have been shown to exhibit some characteristic spatial patterns referred to as resting-state networks. These distinct networks, which are mostly distinguished by their spatial distribution, have been proven to be reproducible via different fMRI data analysis techniques. However, the spatial and temporal interactions in the resting-state fMRI data are merely investigated. It is necessary to investigate the temporal evolution of the "bursts" of activations or the "switching" of different (probably overlapping) networks for better understanding of brain's intrinsic organization. Recently, we have proposed total activation (TA) which reveals the "underlying" activity-patterns in fMRI without incorporating any prior model of the events' onsets and durations. TA is cast as a spatio-temporal regularization where it promotes the sparsity of the innovation signals, which delineate the onsets and offsets of transient activations in each voxel. In this work, we study the temporal and spatial interactions of the synchronized "burst" of activations captured by TA.

***Index Terms*—** fMRI BOLD, spatio-temporal regularization, clustering, synchronous networks, network dynamics

1. INTRODUCTION

Functional magnetic resonance imaging (fMRI) has become an essential tool to visualize the brain function measuring the blood oxygenated level dependent (BOLD) signal during brain activity. In "task-explicit" studies the fMRI data are acquired while subject performs a given task. General linear model (GLM) constitutes the mainstream fMRI data analysis scheme in these studies by fitting a predefined model to the fMRI data. However, in "task-implicit" studies, such as resting-state fMRI, GLM either provides limited information or becomes inapplicable as a model can not be defined a priori.

Immense interest in resting-state fMRI has led to utilization of various methodologies such as seed correlation analysis [1], fuzzy clustering [2], independent component analysis (ICA) [3, 4], temporal correlation analysis [5, 6] and so on. The analysis of temporal and spatial patterns in fMRI data has been an on-going interest. For example, ICA, one of the vastly utilized methods, reveals spatially (temporally) independent sources. Even though the statistical independence would provide well-segregated networks, it is still not clear how the interactions between these components evolve over time. Moreover, the information flow in the components and perhaps the overlapping and distinct spatio-temporal interactions of brain regions should still be further investigated. Recently, the combination of spatial and temporal ICA has been applied to fast fMRI data to study the dynamics of overlapping components [7]. Another interesting method employs a two step clustering analysis to detect the transient activations in fMRI [8].

We have recently proposed a new approach based on spatio-temporal regularization, termed total activation (TA), to extract the "underlying" activity-inducing signals from fMRI data without using any predefined information about the onset and duration of the paradigm. Specifically, in temporal domain, TA applies generalized total variation regularization that incorporates a general differential operator to invert the hemodynamic response. The resulting activity-inducing signals are designed to be built up of block-like signals where the "sparse" innovation signals determine the onsets and offsets of the activations. An additional spatial regularization term promotes smooth but well segregated activations between anatomically defined regions by imposing mixed-norm constraint. Essentially, these properties enables TA to monitor the "underlying" activation patterns also in resting-state fMRI.

In this work, using TA, we investigate the synchronous network dynamics in resting-state fMRI data of 10 healthy subjects. The "active time points" are defined using the (sparse) innovation signals that reflect the "bursts" of transient activity. Then, we perform k-means clustering and project each cluster onto the original time series. The results show that innovation signals are able to disentangle overlapping networks. Moreover, the correlation analysis highlight spatially overlapping networks with distinct temporal patterns.

2. METHODS

2.1. Total Activation

TA recovers the "underlying" activity-inducing signals from noisy fMRI measurements by incorporating a differential operator that inverts the hemodynamic effect. We formulate the measured fMRI BOLD signal of the i^{th} voxel $y[i,t]$ as follows

$$y[i,t] = u[i,t] * h[t] + \epsilon[i,t] = x[i,t] + \epsilon[i,t], \quad (1)$$

$$\Delta_{L_h}\{x[i,\cdot]\}[t] = u[i,t], \quad \Delta_L\{x[i,\cdot]\}[t] = u_s[i,t], \quad (2)$$

where $h[t]$ is the hemodynamic response function, that is the Green's function of derivative operator $\Delta_{L)h}$, $u[i,t]$ is the activity-inducing signals, ϵ is white Gaussian noise, $u_s[i,t]$ is the innovation signal,

This work was supported in part by the Swiss National Science Foundation (under grants PP00P2-146318 and 51AU40-125759) and in part by EPFL BMI-HU collaboration grant, Center for Biomedical Imaging (CIBM) of the Geneva-Lausanne Universities, and National Center of Competence in Research.

$\Delta_L = \Delta_D \Delta_{L_h}$, and Δ_D is the first order differential operator. The differential operator is adapted from the formulation in [9] based on the first-order Volterra series approximation of non-linear Balloon model [10, 11].

TA is cast as a convex problem imposing (structured)-sparsity priors in the spatiotemporal domain. It incorporates spatial and temporal regularization terms; the former uses a mixed-norm constraint to promote coherent activations inside anatomically defined regions whereas sparse activations across the volume, and the latter exploits the sparsity of the innovation signal. Combining these two constraints with a least-squares data fitting term, we solve for the following regularization problem

$$\tilde{\mathbf{x}} = \arg\min_{\mathbf{x}} \frac{1}{2}\|\mathbf{y} - \mathbf{x}\|_F^2 + \mathcal{R}_T(\mathbf{x}) + \mathcal{R}_S(\mathbf{x}), \tag{3}$$

where

$$\mathcal{R}_T(\mathbf{x}) = \sum_{i=1}^{V} \lambda_1[i] \underbrace{\|\Delta_L\{\mathbf{x}[i,\cdot]\}\|_1}_{\sum_{t=1}^{N}|\Delta_L\{x[i,t]\}|}, \tag{4}$$

and

$$\mathcal{R}_S(\mathbf{x}) = \sum_{t=1}^{N} \lambda_2[t] \underbrace{\|\Delta_{\text{Lap}}\{\mathbf{x}[\cdot,t]\}\|_{(2,1)}}_{\sum_{k=1}^{M}\sqrt{\sum_{i\in \mathrm{R}_k}\Delta_{\text{Lap}}\{x[i,t]\}^2}}, \tag{5}$$

where Δ_L is the generalized derivative operator that recovers the innovation signals (over time), Δ_{Lap} is the Laplacian operator (over space), λ_1 and λ_2 are the regularization parameters, $||\mathbf{x}||_F$ is the Frobenius norm. λ_1 is tuned automatically according to the estimated noise level of each voxel [17] and λ_2 is picked as 5 empirically.

We employ generalized forward-backward splitting [12], for denoising case also known as parallel Dykstra-like proximal algorithm [13], to solve the optimization problem in (3). The joint solution is obtained by incorporating the proximal maps of both spatial and temporal regularizations [14–17].

2.2. Dynamic Analysis

2.2.1. Synchronous Activations

TA provides a 4D dataset comprising the activity-inducing signals of each voxel. Here, we perform a temporal clustering analysis in order to further investigate the temporal characteristics of the activity-inducing signals. Specifically, we are interested in revealing the synchronized activation patterns and their dynamics. For this purpose, we first computed the average innovation signals of each anatomically defined region in the AAL atlas and "smooth" the innovation signals over time by convolving the time series with a window of length 3 TRs so that small shifts of the hemodynamic response are taken into account. We apply the same steps to the activity-inducing signals $u[i,t]$. Then, we form a subset of the innovation signals that are composed of the onset times of the "positively activate" regions. The subset of the onsets that is kept for further analysis is determined by thresholding the cumulative innovation signals at each time point such that half of the positive activations are preserved,

$$\bar{u}_s[k,t] = \sum_{i\in \mathrm{R}_k} u_s[i,t]\, b[u_s[i,t]], \tag{6}$$

$$t_{on} = \{t : \sum_k \bar{u}_s[k,t] > \Theta\}, \tag{7}$$

$$\tilde{u}_s[k,t] = \{\bar{u}_s[k,t], t \in t_{on}\}, \tag{8}$$

where $\bar{u}_s[k,t]$ are the region-averaged "positive" innovation signals of region k, $b[l] = l, l > 0$ and 0 otherwise, and Θ is the 50% threshold (median). Fig. 1(a) shows the average activity-inducing signal computed for one brain region, posterior cingulate cortex (PCC), and the corresponding "positive" innovation signal, $\bar{u}_s$. Fig. 1(b) depicts the total innovation signal of all regions, $\sum_k \bar{u}_s[k,t]$, and the subset of onsets, t_{on}, kept for clustering analysis.

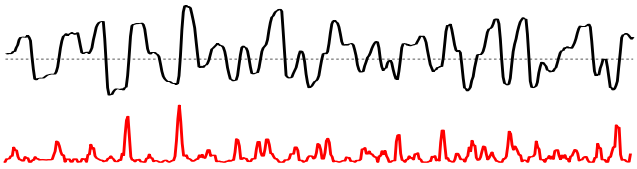

(a) The average activity-inducing signal (black) and positive innovation signal (red) of PCC

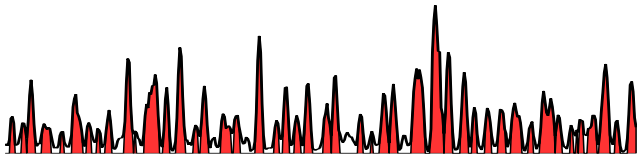

(b) The total innovation signal for all regions (black) and selected time points (red shaded areas)

Fig. 1: Total activation (TA) results, (a) activity-inducing (black) and innovation signals (red) obtained with TA for one region (PCC), and (b) selected time points (50 %, red shaded) to be further used in clustering analysis.

2.2.2. K-means Clustering

We employ k-means clustering to the innovation signals at selected time points, $\tilde{u}_s$, using correlation as a similarity measure. Each time point in the onset subset t_{on} is assigned to the most probable cluster. Instead of extracting the cluster centroids, which are affected by global normalization, we compute the mean activation map of each cluster C_l by averaging the volumes at the time points obtained by clustering.

$$C_l[k] = \frac{1}{|t_{on}[l]|} \sum_{t\in t_{on}[l]} \tilde{u}_s[k,t], \tag{9}$$

where $|\cdot|$ represents cardinality.

2.2.3. Least Square Fitting

Performing the cluster analysis on the innovation signals enables to capture the transient activity that are potentially lost in the block-like activity-inducing signals due to integration and superposition of temporally overlapping networks. Here, we backproject the clusters on activity-inducing signals to monitor these transient activations that are captured from the innovation signal. We employ a linear regression as

$$\hat{\boldsymbol{\beta}} = \arg_{\boldsymbol{\beta}} \min \|\mathbf{u} - \mathbf{X}\boldsymbol{\beta}\|_2^2, \tag{10}$$

where each column of regressor $\mathbf{X}$ is a cluster map $C_l[k]$ normalized by its ℓ_2-norm, and $\mathbf{u}$ are the activity-inducing signals. The $\boldsymbol{\beta}$ values reveal the contribution of each cluster in the activity-inducing signals temporally.

3. RESULTS

3.1. Resting-State FMRI Data

We analyze the resting-state fMRI data of 10 healthy subjects who are requested to lie in the scanner with their eyes are closed. The fMRI data were acquired on a Siemens 3T TrioTIM using gradient-echo planar imaging (TE = 27 ms, TR = 1.1 s, flip angle = 90^o, matrix = 64 $\times$ 64, 21 transverse slices, voxel size = 3.75 $\times$ 3.75 $\times$ 5.63 mm^3, 450 volumes). The following preprocessing steps are performed: fMRI volumes were realigned to the first scan and spatially smoothed with Gaussian filter (FWHM=5mm) using SPM8 (FIL,UCL,UK). The anatomical AAL atlas [18] (90 regions without the cerebellum) was mapped onto the subject's functional space using the IBASPM toolbox [19]. The first 10 volumes are discarded and voxels' time series labelled within the atlas were detrended for slow oscillations using a first-degree polynomial and DCT basis function up to cut-off frequency of $1/125$ Hz, and finally scaled to have unit variance.

3.2. Spatially Segregated Clusters

We obtain 15 clusters with k-means clustering. The number of clusters are determined using a cross-validation scheme and the stability of k-means clustering is satisfied by replicating k-means clustering. Fig. 2 shows the cluster maps that are computed by averaging the activation maps in each cluster. The clusters are spatially segregated and localized due to the special encoding of the onsets from innovation signals. Most resting-state networks as well as the subcortical structures are well-distinguished in clusters. Clusters 1, 6, 9 and 11 show the primary and secondary visual areas. Clusters 2, 7 and 12 comprise the anterior and posterior default-mode network (DMN), which are also found to be segregated in previous studies [20]. Some subcortical structures, such as thalamus and putamen, are depicted in cluster 3 and 10. Cluster 4 captures most of the olfactory areas, cluster 5 points the motor areas and cluster 8 represents auditory regions. Cluster 13 includes the supramarginal gyrus, and frontal and parietal attention regions are depicted mostly in clusters 14 and 15.

3.3. Dynamic Mapping

We investigate the clusters and their dynamic patterns by first projecting the clusters into activity-inducing signals (whole time series) via least squares fitting. Then, we compute the temporal correlation between cluster coefficients as well as the spatial correlation between the clusters. The upper and lower triangular part of the correlation matrix in Fig. 3 shows the spatial and temporal correlations, respectively. The correlation values that are closely related to the DMN are depicted by dashed squares. The anterior regions are mostly cumulated in cluster 2 whereas posterior regions are cumulated in cluster 12. Cluster 2 includes both anterior and posterior DMN. We observe that two spatially overlapping DMN clusters, (clusters 2 and 7, clusters 7 and 12) have anti-correlated temporal patterns. On the contrary, the clusters that involve anterior and posterior DMN (cluster 2 and 12) have very small spatial correlation, however, their temporal correlation suggests relatively higher positive correlation. Similar trends exist in visual networks between primary and secondary visual regions (clusters 1,6 and 9) that are depicted by white squares in Fig. 3. These result might suggest the existence of subnetworks with different temporal characteristics or temporal information flow between these clusters; i.e., the clusters are lagging each other. We performed a non-parametric test on the correlation differences where the surrogate data is generated from the random shuffling of the correlation matrix in Fig. 3. Clusters 7 and 12 are depicted as the clusters with significant spatial and temporal correlation difference ($p < 0.05$, corrected).

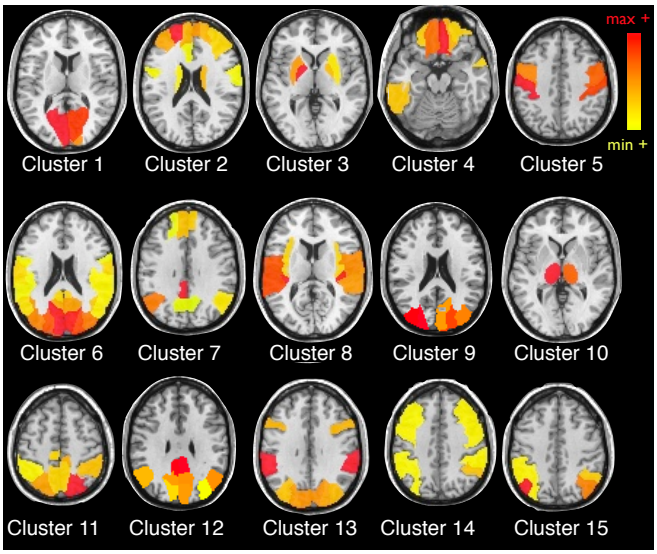

Fig. 2: K-means clustering results, only selected slices of each cluster are shown, the maps are thresholded for visual purposes. The activation maps are obtained by averaging the innovation signals in each cluster. The maps have only positive values since only the positive contributions of the innovation signal are considered in the analysis. The color bar relates to the weights of each region in the corresponding cluster.

4. DISCUSSION AND CONCLUSION

We have recently proposed TA to deconvolve the fMRI time series. TA is cast as a spatiotemporal regularization that reveal block-like activity-inducing signals without any prior on their onset and duration. Moreover, the spatial regularization assures coherent activations inside anatomically defined brain regions. The fundamental assumption of TA is to promote the sparsity of the innovation signal which can disentangle the ongoing activity-inducing signals and inherently capture the fast transient activity. In this work, starting from the innovation signals, we elaborate both temporal and spatial characteristics of these "bursts" of transient activity in resting-state fMRI. The clusters were obtained on group level using only a subset of onsets in the innovation signals. The clusters unveiled spatially well-segregated networks that are typically encountered in other resting-state fMRI studies. The back projection of the clusters into the underlying activity-inducing signals enabled to monitor the ongoing temporal dynamics and interactions of these clusters. We compared the spatial and temporal correlations of clusters and found a negative trend between these correlations. Clusters that are involved in well-know resting-state networks (visual network and DMN) exhibited distinct temporal patterns although they spatially coincide.

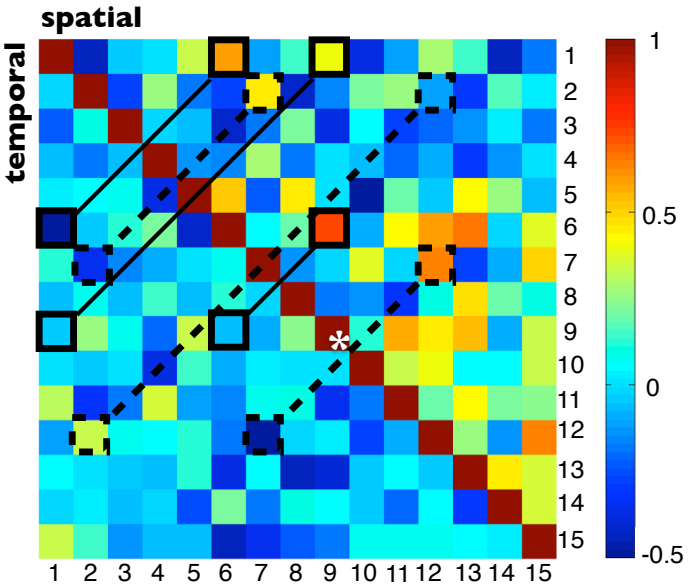

Fig. 3: The spatial and temporal correlation matrix. Upper triangle shows the spatial correlation of each cluster and lower triangular shows the temporal correlation of least squares fitting parameters, β, for each cluster. The correlation between clusters 2, 7, and 12 reveals the spatially overlapping(segregated) but temporally anti-correlated(correlated) DMN regions (dashed black). The correlations between overlapping visual networks (clusters 1, 6 and 9) also reveal temporally distinct patterns (black). We perform a non-parametric hypothesis testing to delineate the significant differences between temporal and spatial correlations; the correlation difference between clusters 7 (full DMN) and 12 (posterior DMN) are determined as significant (starred, $p < 0.05$, corrected).

5. REFERENCES

[1] B. Biswal, F. Z. Yetkin, V.M. Haughton, and J.S. Hyde, "Functional connectivity in the motor cortex of resting human brain using echo-planar MRI.," *Magnetic Resonance in Medicine*, vol. 34, no. 4, pp. 537–541, Oct. 1995.

[2] R Baumgartner, L Ryner, W Richter, R Summers, M Jarmasz, and R Somorjai, "Comparison of two exploratory data analysis methods for fMRI: fuzzy clustering vs. principal component analysis," *Magnetic Resonance Imaging*, vol. 18, no. 1, pp. 89 – 94, 2000.

[3] C. F. Beckmann and S. M. Smith, "Probabilistic independent component analysis for fMRI," *IEEE Transactions on Medical Imaging*, vol. 23, no. 2, pp. 137 –152, feb. 2004.

[4] V.D. Calhoun and T. Adali, "Unmixing fMRI with independent component analysis," *IEEE Engineering in Medicine and Biology Magazine*, vol. 25, no. 2, pp. 79 – 90, march-april 2006.

[5] Y. Liu, J.-H. Gao, H.-L. Liu, and P. T. Fox, "The temporal response of the brain after eating revealed by functional MRI," *Nature*, vol. 405, pp. 1058–1062, 2000.

[6] V. L. Morgan, Y. Li, B. Abou-Khalil, and J. C. Gore, "Development of 2dTCA for the detection of irregular, transient BOLD activity," *Human Brain Mapping*, vol. 29, no. 1, pp. 57–69, 2008.

[7] S. M. Smith, K. L. Miller, S. Moeller, J. Xu, E. J. Auerbach, M. W. Woolrich, C. F. Beckmann, M. Jenkinson, J. Andersson, M. F. Glasser, D. C. Van Essen, D. A. Feinberg, E. S. Yacoub, and K. Ugurbil, "Temporally-independent functional modes of spontaneous brain activity," *Proceedings of the National Academy of Sciences*, vol. 8, pp. 3131–3136, 2012.

[8] Cecile Bordier and Emiliano Macaluso, "Detection of transient inter-regional coupling in fmri time series: A new method combining inter-subjects synchronization and cluster-analyses," in *Pattern Recognition in Neuroimaging (PRNI), 2013 International Workshop on*, 2013, pp. 119–123.

[9] I. Khalidov, J. Fadili, F. Lazeyras, D. Van De Ville, and Michael Unser, "Activelets: Wavelets for sparse representation of hemodynamic responses," *Signal Processing*, vol. 91, no. 12, pp. 2810–2821, 2011.

[10] K. J. Friston, A. Mechelli, R. Turner, and C. J. Price, "Nonlinear responses in fMRI: The balloon model, Volterra kernels, and other hemodynamics," *NeuroImage*, vol. 12, no. 4, pp. 466 – 477, 2000.

[11] R. B. Buxton, E. C. Wong, and L. R. Frank, "Dynamics of blood flow and oxygenation changes during brain activation: The Balloon model.," *Magnetic Resonance in Medicine*, vol. 39, no. 6, pp. 855–864, Jun 1998.

[12] H. Raguet, J. Fadili, and G. Peyrè, "Generalized forward-backward splitting," 2012, Available [Online], arxiv.org/abs/1108.4404v3.

[13] P.L. Combettes, "Iterative construction of the resolvent of a sum of maximal operators," *Convex Analysis*, vol. 16, pp. 727–748, 2009.

[14] J.-C. Baritaux, K. Hassler, M. Bucher, S. Sanyal, and M. Unser, "Sparsity-driven reconstruction for FDOT with anatomical priors," *IEEE Transactions on Medical Imaging*, vol. 30, no. 5, pp. 1143–1153, May 2011.

[15] A. Beck and M. Teboulle, "Fast gradient-based algorithms for constrained total variation image denoising and deblurring problems," *IEEE Transactions on Image Processing*, vol. 18, no. 11, pp. 2419–2434, Nov. 2009.

[16] A. Chambolle, "An algorithm for total variation minimization and applications," *Journal of Mathematical Imaging and Vision*, vol. 20, no. 1, pp. 89–97, January 2004.

[17] F. I. Karahanoglu, C. Caballero-Gaudes, F. Lazeyras, and D. Van De Ville, "Total activation: fMRI deconvolution through spatio-temporal regularization," *NeuroImage*, vol. 73, pp. 121 – 134, 2013.

[18] N. Tzourio-Mazoyer, B. Landeau, D. Papathanassiou, F. Crivello, O. Etard, N. Delcroix, B. Mazoyer, and M. Loliot, "Automated anatomical labeling of activations in SPM using a macroscopic anatomical parcellation of the MNI MRI single-subject brain," *NeuroImage*, vol. 15, pp. 273–289, 2002.

[19] Y. Alemán-Gómez, L. Melie-Garćia, and P. Valdés-Hernandez, "IBASPM: Toolbox for automatic parcellation of brain structures," *12th Annual Meeting of the Organization for Human Brain Mapping*, vol. 27, 2006.

[20] D. Van De Ville, P. Jhooti, T. Haas, R. Kopel, K.-O. Lovblad, K. Scheffler, and S. Haller, "Recovery and spatio-temporal segregation of default mode subnetworks," *NeuroImage*, vol. 63, no. 4, pp. 1175–1781, 2012.